

*Letter to the Editor***Stellar dynamics observations of a double nucleus in M 83**N. Thatte<sup>1</sup>, M. Tecza<sup>1</sup>, and R. Genzel<sup>1</sup>

Max-Planck-Institut für extraterrestrische Physik, Giessenbachstrasse, 85748 Garching, Germany (thatte@mpe.mpg.de)

Received 17 August 2000 / Accepted 4 September 2000

**Abstract.** We report on the discovery of a double nucleus in M 83, based on measurements of the line of sight velocity distribution of stars observed at near infrared wavelengths with the VLT ISAAC spectrograph. We observe two peaks separated by  $2''.7$  in the velocity dispersion profile of light from late-type stars measured along a slit  $0''.6$  wide, centered on the peak of K band emission and with P.A.  $51.7^\circ$ . The first peak coincides with the peak of the K band light distribution, widely assumed to be the galaxy nucleus. The second peak, of almost equal strength, almost coincides with the center of symmetry of the outer isophotes of the galaxy. The secondary peak location has little K band emission, and appears to be significantly extinguished, even at near infrared wavelengths. It also lies along a mid-infrared bar, previously identified by Gallais et al. (1991) and shows strong hydrogen recombination emission at  $1.875\mu\text{m}$ . If we interpret the observed stellar velocity dispersion as coming from a virialized system, the two nuclei would each contain an enclosed mass of  $13.2 \times 10^6 M_\odot$  within a radius of 5.4 pc. These could either be massive star clusters, or supermassive dark objects.

**Key words:** galaxies: kinematics and dynamics – galaxies: nuclei – galaxies: individual: M 83 – galaxies: spiral – galaxies: starburst – galaxies: stellar content – galaxies: structure

**1. Introduction**

M 83 is a very nearby grand design barred spiral (Hubble type SAB(s)c, distance 3.7 Mpc, de Vaucouleurs et al. 1991) showing vigorous star forming activity in its nuclear region. It has been the object of numerous studies at all wavelengths, ranging from the X-ray (Immler et al. 1999), visible (Sofue and Wakamatsu 1994; Comte 1981), near-infrared (Gallais et al. 1991), mid-infrared (Telesco, Dressel and Wolstencroft 1993; Rouan et al. 1996), to the radio (Ishizuki 1993). Significant dust extinction in the nuclear region (Turner, Ho and Beck 1987) implies that the true morphology of the starburst is revealed only at infrared and longer wavelengths.

---

Send offprint requests to: N. Thatte

Although the morphology of the nuclear star forming activity has been studied in detail, very few kinematic or dynamical studies at arc second resolution have been carried out. Radio measurements exist, but are hampered by the large beam size. Puxley, Doyon and Ward (1997) have performed low resolution near infrared spectroscopy along a single slit, characterizing the stellar population in a broad way. As part of a program to search for supermassive black holes in nearby spiral galaxies, we have conducted long slit medium resolution spectroscopy of the nuclear region of M 83 using the ISAAC near infrared spectrometer on the European Southern Observatory's (ESO) Very Large Telescope VLT. Our observations are suggestive of the presence of a double nucleus.

**2. Observations and data reduction***2.1. NTT SOFI imaging*

As part of the near infrared imaging carried out for the supermassive black hole search pilot program, we obtained K band images of the central region of M83 using the SOFI near infrared camera on the ESO NTT telescope. M 83 was observed on 14-15 February 2000 for a total of 600 seconds with the  $K_s$  filter. Individual exposure times were 10 seconds long, grouped together in sets of 12 exposures. Three exposures on blank sky located  $5'$  E of the galaxy nucleus were interposed after every group of on-target exposures. A jitter pattern with a  $20''$  throw in both R.A. and Dec was used to offset every group of on-target exposures relative to the previous one. The seeing was  $0''.9$  during the observations. We used the large field mode of SOFI, with a pixel scale of  $0''.29$  and a total field of view of  $\sim 5' \times 5'$ . The reference star GSPC S791-C was observed a few minutes later for use as a photometric reference.

Data reduction was carried out using the ECLIPSE<sup>1</sup> (Devillard 1999) jitter routines. The process consists of applying dark frame subtraction, flat field division and bad pixel correction to every group of exposures. The source and sky exposures are then input to a dejittering routine which performs sky subtraction, determines the offset between groups and re-centers

---

<sup>1</sup> The ECLIPSE package ([www.eso.org/eclipse](http://www.eso.org/eclipse)) consists of a set of stand alone routines provided by ESO for SOFI and ISAAC data reduction

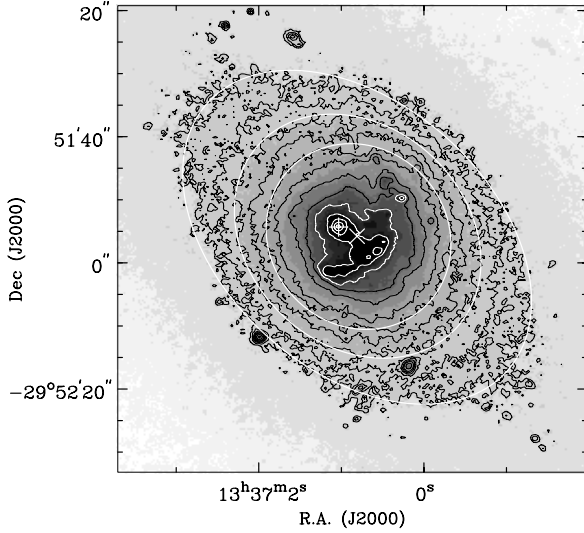


**Fig. 1.**  $K_s$  image of the central region of M 83, obtained with SOFI at the ESO NTT. Grey scale and contour representations are superposed on each other. Contours range from the peak intensity to 5 mag below the peak in steps of 0.25 mag. The plus indicates the location of the photometric peak, while the cross indicates the center of symmetry of the outer isophotes of the galaxy. Fits to the outer isophotes are indicated by white ellipses.

frames, and finally co-adds the frames to yield the reduced image. Fig. 1 shows the  $K_s$  image of the central region of M 83, as observed with SOFI.

## 2.2. VLT ISAAC spectroscopy

We obtained spectra of the nuclear region of M 83 on March 20–21, 2000, using the near infrared spectrometer ISAAC at the VLT. We used two slit positions at position angle (P.A.)  $51.7^\circ$  (major axis) and  $141.7^\circ$  (minor axis). The major axis slit is located along the primary stellar bar whose position angle is measured from the SOFI images. The slit width was set to  $0''.6$  ( $\sim 4$  detector pixels), corresponding to an instrumental resolution of ( $R \equiv \lambda/\Delta\lambda$ ) 4750. The spectral coverage extended from  $2.238\mu\text{m}$  to  $2.361\mu\text{m}$ , with a scale of  $\Delta\lambda = 1.212\text{\AA}$  per pixel. We observed for a total on-source integration time of 4500 seconds per slit setting. Individual exposures were 300 seconds long. We nodded  $30''$  along the slit after each on-target exposure. Due to the large spatial extent of the galaxy which spanned the entire length of the ISAAC slit ( $120''$ ), we nodded the telescope to blank sky  $5'$  E of the galaxy nucleus after every three on-target exposures. The seeing during the observations varied between  $0''.7$  and  $1''.1$ . The star HD 118187 (F7/F8V) was observed as a spectroscopic calibrator on both nights, interleaved with the observations of M 83.

In addition, we obtained spectra of several late type giant stars (spectral types K1III to M5III) for use as spectral templates in the data analysis. Each star was observed using the same slit setting as M 83, and nodded  $30''$  along the slit every 5 to 10 seconds. Details of the template stellar spectra will be presented in a subsequent paper.

**Table 1.** Summary of NICMOS archival data

| Dataset name  | Filter | $T_{\text{int}}$ | Feature                       |
|---------------|--------|------------------|-------------------------------|
| N4BV100D0_MOS | F160W  | 48 s             | H band                        |
| N4BV100K0_MOS | F187N  | 160 s            | Pa $\alpha$                   |
| N4BV100N0_MOS | F190N  | 160 s            | Pa $\alpha$ continuum         |
| N4BV100G0_MOS | F212N  | 576 s            | H <sub>2</sub> S(1)           |
| N4BV100T0_MOS | F215N  | 576 s            | H <sub>2</sub> S(1) continuum |
| N4BV100X0_MOS | F222M  | 176 s            | K band                        |

We dark subtracted, flat-fielded and dead pixel corrected each spectroscopic exposure, and then transformed it onto a linear wavelength grid with dispersion axis precisely parallel to detector rows. Our sky subtraction was done using *smoothed sky* exposures so as not to degrade the signal to noise ratio (SNR). We smoothed each sky spectrum over 100 spatial pixels while maintaining the small scale spatial structure along the slit, to produce the smoothed sky. The results yielded useful galaxy spectra over the entire slit length with better SNR than using standard *nodding-on-slit* techniques. Atmospheric transmission corrections were made by dividing the sky subtracted, co-added galaxy spectra by spectra of the spectroscopic reference star, thus eliminating the only significant telluric absorption feature at  $2.317\mu\text{m}$ . Finally, a second interactive dead pixel correction was employed to tag any hot or transient pixels. The continuum for each spatial pixel along the slit was normalized to unity over the wavelength range  $2.255 - 2.300\mu\text{m}$ , excluding the Ca feature at  $2.265\mu\text{m}$ .

The template star spectra were reduced in a manner similar to the galaxy spectra, with the exception that sky subtraction was performed by subtracting two nodded exposures from each other, shifting the positive maxima so that they overlay, and co-adding the data. A single spectrum was extracted for each template star using the *apall* routine within the *twodspec* package of IRAF.

## 2.3. Archival HST NICMOS images

We supplemented our broad band ground based images and medium resolution spectra with archival data from the HST NICMOS camera. (P.I. M. Rieke, Proposal I.D. 7218). In particular, we used 6 datasets obtained with the NIC2 camera, taken on 16 May 1998. Table 1 lists the details of the archival data used. The NIC2 camera has a pixel scale of  $0''.075$ , corresponding to a total field of view of  $19''.2 \times 19''.2$ . The observations were made in mosaic mode using multiple readouts of the detector for each pointing.

We used pipeline calibrated data from the STSCI archive, processed by both the *calnica* and *calnicb* pipelines. These pipelines together provide dead pixel and cosmic ray correction, flat fielding, dark subtraction, photometric calibration and co-addition of individual pointings of a mosaic into a single image. We used the photometric  $F_\nu$  calibration, together with H and K zero points (Cox 2000) to establish a flux scale (in magnitudes) for the F160W and F222M images and to yield a

H-K color map. Fig. 2 shows the F222M NICMOS image of the nuclear region of M 83, with the H-K color overlaid in contours. Both the H and K images were smoothed prior to subtraction with a two dimensional Gaussian with  $\sigma = 0''.150$ , so as to mitigate artifacts arising from the different point spread functions at the two wavelengths. The resulting H-K map still shows a residual weak depression in the H-K color at the location of every strong point source.

### 3. Analysis and results

#### 3.1. Isophote fits: the location of the photometric centroid

We used the ELLFIT routine with the GIPSY<sup>2</sup> (van der Hulst et al. 1992) package to perform elliptical isophote fits to the K band surface brightness distribution observed with SOFI. We fit points within a magnitude interval ranging from 5.00 to 3.75 of the peak intensity, with a width of 0.25 magnitudes for each fit, and a step size of 0.25 magnitudes. All fit parameters for the ellipses were unconstrained. Fig. 1 shows some of the isophotal fits overlaid on a contour and grey scale image of the central region of M 83. The center of symmetry obtained from the fits lies  $1''.54 \pm 0''.27$  South and  $3''.05 \pm 0''.30$  West of the photometric peak. Wolstencroft 1988 also observed a similar offset ( $3''$  at P.A.  $255^\circ$ ) based on lower resolution K band data. At larger spatial scales ( $\sim 2'$ ), the bar is easily identified in the K band image. We measure the positional angle of the bar from the SOFI image to be  $51.7^\circ \pm 1^\circ$ .

#### 3.2. Recession velocity and velocity dispersion: discovery of a hidden nucleus

We used both Fourier correlation quotient and  $\chi^2$  fitting techniques to determine the recession velocity and the velocity dispersion as a function of slit position.

The reduced ISAAC data provided a normalized spectrum for each spatial pixel along the slit. We binned the spectra along the spatial direction with a binning width of four pixels (equal to the slit width), yielding spectra with enhanced SNR spaced every  $0''.6$  along the slit. The total spatial extent of the major axis slit used for dynamical analysis was  $\sim 13''$ , based on an SNR cutoff of 20 per pixel in the continuum. Fig. 3 shows some representative galaxy spectra around the region of the CO  $0 \rightarrow 2$  bandhead feature at  $2.29 \mu\text{m}$ , as well as a spectrum of a template star for comparison.

We measured the redshift and velocity dispersion as a function of spatial position along the slit by fitting a suitably broadened and shifted template stellar spectrum to the galaxy spectrum. The normalized galaxy and template star spectra were resampled onto a grid with equispaced velocity intervals (corresponding to logarithmic intervals in wavelength). The template star spectrum was convolved with a Gaussian broadening function whose width and mean velocity were free parameters. A least squares fit, minimizing the normalized mean square er-

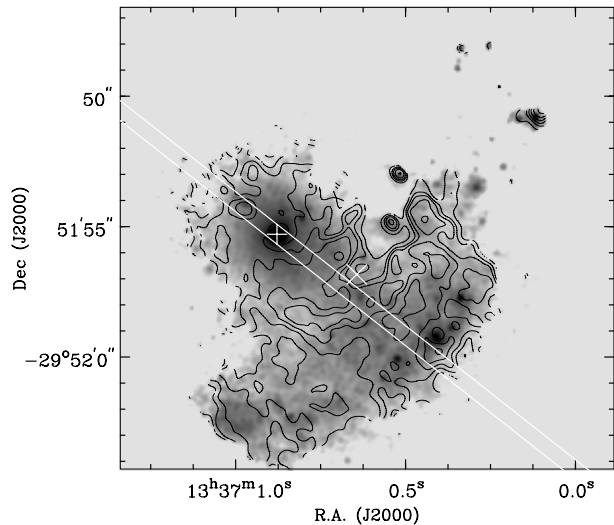


**Fig. 2.** NICMOS  $2.22 \mu\text{m}$  image of the nuclear region of M 83 (grey scale in magnitude units), with contours representing the H-K colour overlaid. Contours are at 0.2, 0.3, 0.4, 0.5, 0.6 and 0.8 magnitudes. The locations of the major axis slit used for ISAAC spectroscopy, are also indicated. A cross indicates the location of the center of symmetry of the outer isophotes of the galaxy.

ror,  $\chi^2$ , between the broadened template star spectrum and the galaxy spectrum yielded the best fit values for the recession velocity and velocity dispersion. The range of the fit was optimized to include all significant spectral features (CO bandheads and Ca absorption lines) and a minimum of line-free continuum. The lack of continuum longward of the CO bandhead features can lead to incorrect estimates of the continuum level. Consequently, we also included a quadratic polynomial term to account for a mismatch in the continuum levels of the two spectra.

A thorough error analysis was carried out estimating both systematic errors (due to template mismatch) and random errors resulting from noise in the galaxy spectra. Systematic errors were estimated using template stars of varying spectral type (K3III to M2III) for the fit and measuring the observed differences in fit velocities and dispersions. Random errors were estimated using a reduced  $\chi^2$  technique. Artificially broadened template star spectra with added random noise (to appropriately mimic the observed SNR of the galaxy spectra) were fitted as described above. The change in fit parameters required to increase the reduced  $\chi^2$  by unity is a measure of the error in each fit parameter. The instrumental resolution corresponds to a  $\sigma$  of  $27 \text{ km s}^{-1}$ , and represents the limit of what can be resolved by these observations.

Fig. 4 shows the results of the  $\chi^2$  fitting for the major axis of M 83. A velocity dispersion peak is coincident with the location of the K band photometric peak, believed to be the nucleus. We also observe a second velocity dispersion peak, of equal strength, offset  $2''.7$  south-west from the nucleus (see Fig. 3 for a comparison of broadened CO bandhead profiles at the two peaks). The photometric peak is also associated with a sharp gradient in recession velocity, while no such jump is observed at the location of the secondary peak. The off-nuclear veloc-

<sup>2</sup> The Groningen Image Processing SYstem

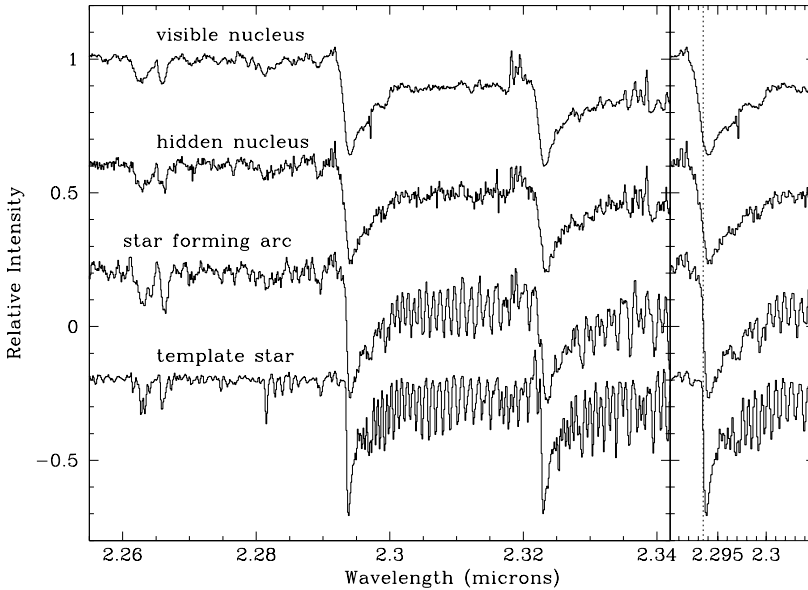


**Fig. 3.** ISAAC spectra of the visible nucleus, hidden nucleus, star forming arc and a template star of type K5III (top to bottom), each within a  $0''.6$  aperture. The galaxy spectra have been shifted to zero redshift. Every spectrum has an amplitude offset of  $-0.4$  relative to the one above it. The resolved CO lines between  $2.30$  and  $2.32\mu\text{m}$  are very sensitive indicators of velocity dispersion. An expanded view of the region around the  $^{12}\text{CO}$  bandhead at  $2.293\mu\text{m}$  is shown on the right. The velocity broadening toward both nuclei is clearly seen.

ity dispersion peak could possibly be a second nucleus, hidden from our view at visible and near infrared wavelengths due to significant extinction. We elaborate on the properties of the second nucleus in Sect. 4. The minor axis dynamics shows a single peak at the location of the photometric peak, with no other features. The line of sight recession velocity is remarkably consistent with the velocities of cold molecular gas observed by Handa et al. 1990. For a galaxy inclination of  $24^\circ$  to face-on (Comte 1981), the deprojected rotation velocities are a factor of 2.46 higher than the observed values.

We also analyzed the major and minor axis spectra using the Fourier cross correlation quotient method. The technique is described by Bender 1990, and has been shown to work equally well for asymmetric line profiles, such as the  $^{12}\text{CO}$  bandhead by Anders 1999, Tecza 1999 and others. Essentially, it consists of deconvolving the galaxy spectrum using an appropriate template star spectrum, so as to yield the line of sight velocity distribution (LOSVD) for each spatial resolution element. The deconvolution is achieved by cross-correlating the galaxy spectrum with the stellar spectrum, and dividing the result with the auto-correlation of the stellar spectrum. The convolutions are carried out in Fourier space, and a Wiener filter is used to limit the high frequency component of the result, so as to minimize noise amplification.

The Fourier cross correlation quotient (FCQ) technique is superior to a simple deconvolution since it suppresses those frequencies in the result where the template stellar spectrum contains little or no information. It has the additional advantage that it is relatively insensitive to *template mismatch*. The latter occurs when the spectral type of the template does not match that of the galaxy spectrum being deconvolved. The depth of the CO bandhead features is a function of spectral type and luminosity class (Oliva et al. 1995), and  $\chi^2$  fitting techniques are prone to interpreting a deeper template feature as high velocity dispersion in the galaxy spectrum, and vice versa. FCQ techniques also make no assumption regarding the LOSVD being observed. The

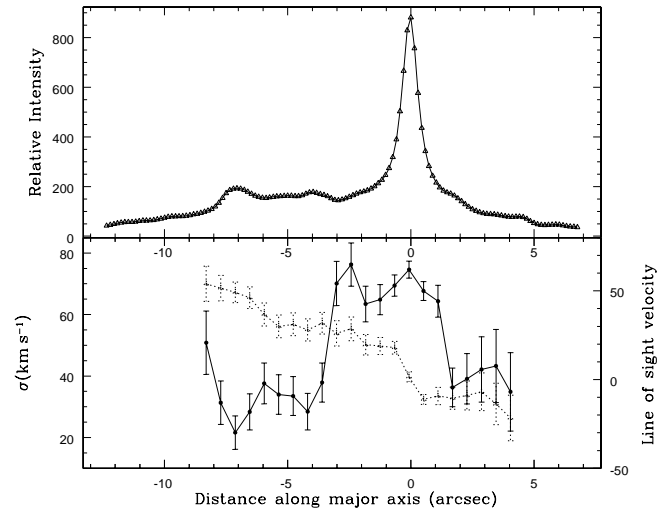


**Fig. 4.** Photometric and kinematic profiles along the major axis of M 83. The top plot shows the intensity for a  $0''.6$  slit at P.A.  $51.7^\circ$  as a function of offset from the location of the visible nucleus. Positive offsets are toward the north-east. The bottom plot shows the recession velocity (dotted line and triangles) and line of sight velocity dispersion (solid line and circles) as determined by comparison with a stellar template over the wavelength range  $2.26 - 2.34\mu\text{m}$ , using a  $\chi^2$  fit. Error bars represent  $3\sigma$  uncertainties including both systematic and random errors. The secondary nucleus is evident as a second dynamical peak which roughly matches the dip in the K band light profile. The visible nucleus is also associated with a sharp gradient in the recession velocity.

disadvantage of the FCQ technique is that it requires higher SNR spectra, precisely because it makes no apriori assumptions about the LOSVD. A cross-check of our dynamical analysis using FCQ techniques assuming a Gaussian LOSVD yielded almost identical results to those presented in Fig. 4. Single component, broad LOSVDs were observed at the location of both dynamical peaks.

**Table 2.** Magnitudes and colors for emission peaks

| Source name | $\Delta$ RA from 1   | $\Delta$ Dec from 1 | $m_K$ (r=5 pix) | $m_H$ (r=5 pix) | $A_V$ |
|-------------|----------------------|---------------------|-----------------|-----------------|-------|
| 1           | 0 <sup>h</sup> :00   | 0 <sup>m</sup> :00  | 12.31           | 12.63           | 0.9   |
| 3           | -0 <sup>h</sup> :039 | -7 <sup>m</sup> :03 | 15.27           | 15.56           | 0.5   |
| 4           | -0 <sup>h</sup> :359 | -4 <sup>m</sup> :76 | 14.44           | 14.86           | 2.5   |
| 5a          | -0 <sup>h</sup> :473 | -4 <sup>m</sup> :00 | 13.40           | 13.83           | 2.6   |
| 5b          | -0 <sup>h</sup> :521 | -3 <sup>m</sup> :55 | 14.22           | 14.73           | 3.8   |
| 6a          | -0 <sup>h</sup> :771 | 4 <sup>m</sup> :57  | 13.86           | 14.35           | 3.5   |
| 6b          | -0 <sup>h</sup> :723 | 4 <sup>m</sup> :48  | 14.60           | 15.30           | 6.7   |
| 8           | -0 <sup>h</sup> :595 | 1 <sup>m</sup> :86  | 14.59           | 15.45           | 9.2   |
| 9           | -0 <sup>h</sup> :547 | -2 <sup>m</sup> :40 | 14.03           | 14.44           | 2.3   |
| 10          | -0 <sup>h</sup> :333 | 0 <sup>m</sup> :50  | 15.32           | 15.67           | 1.4   |

### 3.3. Stellar population analysis: extinction and luminous mass estimates

#### 3.3.1. Magnitudes and colors

We have derived K band magnitudes for the nucleus, several star forming knots within the near infrared arc, and points along the mid infrared bar, based on the calibrated NICMOS K band image. A radial profile analysis of several of the star forming knots yielded a FWHM of  $\sim 3$  pixels ( $0''.225$ ), consistent with the diffraction limit at  $2.2 \mu\text{m}$ . Consequently, we used an aperture with a radius of 5 pixels for our aperture photometry. The observed K band magnitudes, and positions relative to the photometric peak of several knots are listed in Table 2. We adopt the nomenclature of Gallais et al. 1991, further extended by Elmegreen, Chromey and Warren 1998, for consistency. Note, however, that source 5 (location of SN 1968L, Wood and Andrews 1974) is resolved into two knots, 5a and 5b, by NICMOS, and source 6 (also referred to as source B by Gallais et al. 1991) also splits up into two sources 6a and 6b at HST resolution. Source 9 corresponds to compact emission  $\sim 2''$  north-west of source 5, which is only detected in the high resolution NICMOS images.

The H-K colours listed in Table 2 have been corrected for a Galactic extinction corresponding to  $E(J-K)=0.017$  mag (de Vaucouleurs et al. 1991). Comparing the observed colours with those expected for an M type giant/super-giant population ( $H-K=0.25$  Koornneef 1983), and assuming a screen model for dust extinction following the standard Galactic law (Cox 2000), we find that the extinction varies over a wide range within the nuclear region.

The nucleus and the southern part of the star forming arc appear only slightly extinguished, with increasing extinction toward the south-west part of the star forming arc. Source 6 (10 micron source B) shows a very strong extinction gradient from 6a to 6b, leading us to postulate that we are only observing a small part of the star forming activity which occurs close to the near edge of the cloud. Source 8 (10 micron source A) shows the highest extinction, consistent with the conclusion of Gallais et al. 1991 that it is younger than B. Most of the region identified as the mid infrared bar by Gallais et al. 1991 is severely extinguished ( $A_V \sim 10$  mag, see also Turner et al. 1987), including the location of

the secondary nucleus. The high extinction is hiding most of the star formation activity within the bar from our view, even at near infrared wavelengths. The NICMOS Pa  $\alpha$  image shows very strong emission all along the mid infrared bar, with a peak located near source 10 (Table 2), confirming the presence of a large number of ionizing photons within the region. The Pa  $\alpha$  emission peak also corresponds to an H  $\alpha$  peak observed in HST WFPC narrow band images (archival data, P.I. S. Heap, Proposal I.D. 1213). Ishizuki (1993) observed a large concentration of cold molecular gas (map published by Sofue and Wakamatsu 1994) in the nuclear region of M 83, with a peak located in the close vicinity of the mid infrared bar.

#### 3.3.2. Equivalent width, age and luminosity

Amongst all the K band emission peaks identified by Gallais et al. 1991 and mentioned in Table 2, only the nucleus (source 1) lies within our major and minor axis slits. We measure an equivalent width for the  $^{12}\text{CO}$  bandhead of  $10.4 \pm 0.4 \text{ \AA}$  at the nuclear location, using the range  $2.2931 - 2.2983 \mu\text{m}$ , as defined by Kleinmann and Hall 1987 (also used by Origlia, Moorwood, and Oliva 1993). Origlia et al. (1993) derive a correction for the observed equivalent width as a function of the velocity dispersion of the source. We have carried out a similar calibration for the ISAAC spectra at  $R \sim 4750$ . We artificially broadened template star spectra using a Gaussian broadening function with widths varying from  $\sigma = 0$  to  $250 \text{ km s}^{-1}$ . We then measured the CO equivalent width over the specified bandpass. A linear least squares fit to the observed variation of equivalent width with velocity dispersion yields

$$W_{\text{true}} = W_{\text{obs}} \times (1 + 1.91 \times 10^{-3} \sigma). \quad (1)$$

Our calibration does not show any flattening at low  $\sigma$  values, in contrast to the relationship derived by Origlia et al. (1993). We attribute their observed flattening to the lower resolution of their spectra, since a change in equivalent width would only occur if the broadening caused by the velocity dispersion is comparable to the intrinsic instrumental resolution. We derive a corrected nuclear equivalent width of  $11.9 \pm 0.5 \text{ \AA}$ , using our formula and the observed nuclear velocity dispersion (Fig. 4).

We used the population synthesis models by Kovo and Sternberg 1999 to estimate the age of the nuclear star formation activity. We assumed a single burst of star formation decaying exponentially with a scaling time to  $10^6$  years, a Salpeter IMF from 1 to  $100 M_{\odot}$ , and solar metallicity for the modeling. The observed CO equivalent width would correspond to a burst of star forming activity between 25 and 60 million years ago. The observed K band luminosity would correspond a total cluster mass of  $2.5 \times 10^6 M_{\odot}$ , assuming a distance to M 83 of 3.7 Mpc (de Vaucouleurs 1979). The nuclear K band light appears to be dominated by a population of giant stars. We repeated our analysis using the models of Leitherer 1999, obtaining similar results. The observed equivalent width at the secondary nucleus, corrected for velocity dispersion, is  $11.9 \pm 0.5 \text{ \AA}$ , indicative of a giant population with age similar to the visible nucleus.

The star forming arc, in contrast, shows a significantly higher CO equivalent width of  $13.7 \pm 0.5 \text{ \AA}$ . The velocity dispersion at this location  $7''$  from the nucleus along the major axis slit is only  $18 \text{ km s}^{-1}$ , yielding a corrected value of  $14.2 \pm 0.5 \text{ \AA}$ . We conclude that the K band light from the star forming arc is dominated by super-giant stars, although we note that the photometric peak along our major axis slit lies between sources 4 and 5. The large equivalent width also implies a younger age of 10 million years for the starburst in the arc, assuming the same population synthesis model parameters as for the nucleus. The observed very low value of velocity dispersion within the arc is consistent with a picture in which the star forming activity within the arc is very young, and has not reached dynamical equilibrium with the gravitational potential of the galaxy. The K band light we observe is dominated by the super giant stellar population which has an internal velocity dispersion too small to be accurately measured at our instrumental resolution. Gallais et al. 1991 also confirm that the observed colours of the star forming arc are consistent with a reddened giant/supergiant population.

#### 4. The nature of the second nucleus

The two peaks in the stellar velocity dispersion profile correspond to dynamically hot systems, if we assume that the stars used to trace the gravitational potential are dynamically relaxed. It is unlikely that we are seeing a very young (and potentially unrelaxed) star cluster, as the observed equivalent widths are those observed for giant rather than super-giant stars. In any case, a very young cluster would exhibit a very low velocity dispersion, in contrast to the observed peaks. A second possible mechanism to create such dynamical peaks without mass concentrations is via velocity anisotropy (orbit crowding or streaming motions), but such a large effect ( $\text{FWHM} \sim 175 \text{ km s}^{-1}$ ) has not been observed in any galaxy nucleus. M 83 is inclined at  $24^\circ$  to the plane of the sky, making it implausible for any rotation within the galactic plane to cause the observed peak (required deprojected velocity  $430 \text{ km s}^{-1}$ ). We conclude that both peaks likely represent dynamically hot *nuclei*.

If we assume that the stellar system is an isothermal sphere, we derive an enclosed mass of  $1.3 \times 10^7 M_\odot$  within 5.4 pc, using the Jeans equation. The mass estimate is even higher if we use the Virial or Bahcall-Tremaine estimators for a system dominated by a point mass. The observed mass could be either in stars or a dark mass concentration. For the visible nucleus (K band photometric peak), we derive a mass estimate of  $2.5 \times 10^6 M_\odot$  for the stellar component, using population synthesis models. The rest of the mass could conceivably exist as a dark mass. A strong parallel may be drawn with the Milky Way, where Genzel et al. 1996 have observed a central dark mass of  $2.8 \times 10^6 M_\odot$ , and the enclosed mass at a radius of 5 pc is  $1.5 \times 10^7 M_\odot$ .

No such conclusion about the mass concentration at the second nucleus can be made, as it is substantially extinguished and we are unable to make an accurate estimate of its intrinsic K band luminosity. However, we note that the location of the second

nucleus coincides almost exactly with the center of symmetry of the outer isophotes of M 83, which ought to represent the dynamical center of the galaxy.

Telesco et al. (1993) observe a bar like morphology of the mid infrared emission. Elmegreen et al. (1998), using extinction maps, argue for the presence of a bar within a bar, with the inner bar orthogonal to the outer one. Such structures have been predicted and observed in several galaxies (Maciejewski and Sparke 2000, Erwin and Sparke 1999). However, in no case does the inner bar appear to be offset from the nucleus as it does in M 83. Dynamical arguments would place the galaxy nucleus exactly along the inner bar, as is the case for the second nucleus observed by us. The outer dust ring seen by Elmegreen et al. (1998), possibly associated with the inner Lindblad resonance, also appears to be centered on the location of the second nucleus. The visible nucleus might, together with the star forming arc and source B, form a ring of star formation activity centered at the location of the second nucleus.

The nearest normal spiral galaxy, M 31, also shows evidence for a double nucleus (Kormendy and Bender 1999; Statler et al. 1999; Bacon et al. 1994). While the nature and cause of the double nucleus is not well understood, transient phenomenon, such as interaction with a companion, could be responsible (Bacon et al. 1994). Interaction between NGC 5253 and M 83 has been postulated by Wolstencroft 1988, it could also be responsible for triggering the starburst activity in M 83. The nuclear region is also a strong X ray source (Immler et al. 1999), although the spatial resolution available to date is inadequate to identify whether it is associated with either of the two dynamical peaks.

#### 5. Conclusions

We have carried out medium resolution long slit spectroscopy along the major and minor axis of M 83, covering the nuclear region. Using the deep, sharp CO bandhead features longward of  $2.29 \mu\text{m}$ , we have analyzed the dynamics of the stellar population in the nuclear region, measuring the recession velocity and velocity dispersion. The velocity dispersion profile shows two peaks, one located at the photometric peak of K band light, and the other offset  $2''7$  south west of it. Each of the two peaks imply an enclosed dynamical mass of  $1.3 \times 10^7 M_\odot$  within 5.4 pc, if the stellar population is dynamically relaxed. The K band emission observed toward the photometric peak is dominated by light from giant stars, with ages between 25 and 60 million years, estimated using population synthesis models for an instantaneous burst. The estimated total mass of such a stellar cluster is  $2.5 \times 10^6 M_\odot$ .

The off-nuclear dynamical peak might correspond to a mass concentration located at the dynamical center of M 83, as evidenced by the center of symmetry of stellar isophotes. Very little K band emission is observed at the location of the second nucleus. It is likely that it is hidden from our view by  $>10$  magnitudes of extinction, since its position lies within a bar of mid-infrared emission and high extinction. We

postulate that the bar represents gas flowing toward the dynamical center of the galaxy. Star formation triggered within the bar is likely responsible for the observed mid-infrared emission.

*Acknowledgements.* We would like to thank the ESO Paranal staff, especially Jean-Gabriel Cuby and Gianni Marconi, for extensive help with the ISAAC observations. The ESO La Silla and Garching staff deserve credit for carrying out the SOFI observing in service mode. We thank the referee for insightful comments. This research made use of the STSCI HST archive, the ESO ST-ECF archive, and the NED and SIMBAD databases. We thank them all for the support.

## References

- Anders, S., 1999, Ph.D. Thesis, Ludwig Maximilians Universität, Munich
- Bacon, R., Emsellem, E., Monnet, G., and Nieto, J., 1994, *A&A*, 281, 691
- Bender, R., 1990, *A&A*, 229, 441
- Comte, G., 1981, *A&AS*, 44, 1981
- Allen's Astrophysical Quantities, 4th edition, ed. Cox, A. N., New York AIP Press, Springer, 2000
- Devillard, N., 1999, in Proc. of Astronomical Data Analysis Software & Systems VIII, ASP Conference Series, 172, 333
- de Vaucouleurs, G., 1979, *AJ*, 84, 1270
- de Vaucouleurs, G., de Vaucouleurs, A., Corwin, H. Jr., Buta, R., Paturel, G., and Fouque, P., 1991, *Third Reference Catalogue of Bright Galaxies*, Springer, New York
- Elmegreen, D. M., Chromey, F. R., and Warren, A. R., 1998, *AJ*, 116, 2834
- Erwin, D., and Sparke, L., 1999, *ApJ*, 521, L37
- Gallais, P., Rouan, D., Lacombe, F., Tiphène, D., and Vauglin, I., 1991, *A&A*, 243, 309
- Genzel, R., Thatte, N., Krabbe, A., Kroker, H., and Tacconi-Garman, L. E., 1996, *ApJ*, 472, 153
- Handa, T., Nakai, N., Sofue, Y., Hayashi, M., and Fujimoto, M., 1990, *PASJ*, 42, 1
- Immler, S., Vogler, A., Ehle, M., and Pietsch, W., 1999, *A&A*, 352, 415
- Ishizuki, S., 1993, Ph.D. Thesis, University of Tokyo
- Kleinmann, and Hall, D., 1987, *ApJS*,
- Kormendy, J., and Bender, R., 1999, *ApJ*, 522, 772
- Koornneef, J., 1983, *A&A*, 128, 84
- Leitherer, C. et al., 1999, *ApJS*, 123, 3
- Maciejewski, W., and Sparke, L., 2000, *MNRAS*, 313, 745
- Oliva, E., Origlia, L., Kotilainen, J., and Moorwood, A., 1995, *A&A*, 301, 55
- Origlia, L., Moorwood, A., and Oliva, T., 1993, *A&A*, 280, 536
- Puxley, P. J., Doyon, R., and Ward, M. J., 1997, *ApJ*, 476, 120
- Rouan, D., et al., 1996, *A&A*, 315, L141
- Sofue, Y., and Wakamatsu, K., 1994, *AJ*, 107, 1018
- Statler, T., King, I., Crane, P., and Jedrzejewski, R., 1999, *AJ*, 117, 894
- Kovo, O., and Sternberg, A., 1999, in preparation
- Tecza, M., 1999, Ph.D. Thesis, Ludwig Maximilians Universität, Munich
- Telesco, C. M., Dressel, L. L., and Wolstencroft, R. D., 1993, *ApJ*, 414, 120
- Turner, J., Ho, P., and Beck, S., 1987, *ApJ*, 313, 644
- van der Hulst, J., Terlouw, J., Begeman, K., Zwitter, W., and Roelfsema, P., 1992, in Proc. of Astronomical Data Analysis Software and Systems I, ASP Conference Series, 25, 131
- Wolstencroft, R., 1988, in *New Ideas in Astronomy*, eds. Bertola, F., Sulentic, J., and Madore, B., Cambridge University Press, p. 79
- Wood, R., and Andrews, P., 1974, *MNRAS*, 167, 13